OATAO
Open Archive Toulouse Archive Ouverte

Open Archive Toulouse Archive Ouverte (OATAO)

OATAO is an open access repository that collects the work of Toulouse researchers and makes it freely available over the web where possible

This is an author's version published in: http://oatao.univ-toulouse.fr/24436

Any correspondence concerning this service should be sent to the repository administrator: tech-oatao@listes-diff.inp-toulouse.fr

Effect of thermal treatment on mechanical and tribological properties of hybrid coatings deposited by sol–gel route on stainless steel

S. Rahoui *, V. Turq, J.-P. Bonino

Université de Toulouse, Université Paul Sabatier, Institut Carnot CIRIMAT, UMR UPS-INP-CNRS 5085, 118 route de Narbonne, F-31062 Toulouse Cedex 9, France

ARTICLE INFO

ABSTRACT

This paper deals with the effect of thermal treatment on the mechanical and tribological properties of an organic inorganic hybrid coating deposited on stainless steel 430. Organic inorganic coating derived from glycidoxypropyltrimethoxysilane (GPTMS) and aluminum tri sec butoxide Al(OsBu)3 were prepared via sol gel route and deposited by dip coating process with various thicknesses. A preliminary thermal analysis (DTA, TGA) of xerogel obtained by hydrolysis and condensation reaction of sols, highlighted three characteristic domains of temperature (110 200 °C, 250 300 °C, 400 500 °C). When thermal treat ments were applied to the coated stainless steel in these temperature domains, the tribological behavior (wear and friction) underwent strong changes, analyzed from linear ball/plane tribometry. The tribological tests showed a lower friction coefficient and wear after thermal treatment at a temperature in the domain 250 300 °C. In order to explain this phenomenon, xerogel structure was studied from XRD and Raman spectroscopy and correlated to the mechanical and adhesive properties and to the tribological behavior.

1. Introduction

In the field of aeronautic materials, most metals need to be protected against wear and friction, to increase the life time and the efficiency of the equipments. Carbides or oxide coatings are widely used in this aim and two types of process were used to develop these coatings; plasma sprayed for thick coatings [1 4] and physical or chemical vapour depo sition (PVD or CVD) for thin coatings [5 7].

Nowadays, the sol gel process appears as a very promising tech nique. Indeed, sol gel process offers many benefits; it is a low cost pro cess and it is relatively easy to control the deposition parameters. The synthesis of coatings via sol gel processing is also used in many fields of materials engineering. Another benefit of sol gel process is to make coatings with properties depending on the application required. Anti corrosion, thermal barrier, electrochemical and optical sensor are some examples of applications [8 15].

For tribological applications, oxide coatings developed via sol gel process display excellent antiwear and friction performances under low loads [16 18]. Hybrid coatings show interesting properties, such as good adhesion on substrate, flexibility and good coverage [19 21] making them good candidates for various applications. However, hybrid coatings via sol gel route are rarely used for tribological applications.

The aim of this work is to develop hybrid sol gel coating and im prove its tribological properties using a thermal treatment. First, thermal analysis was used to determine temperatures of thermal treatment. Then, coatings and bulk xerogel were thermally treated, and we studied chemical and structural transformations, with XRD and Raman spectroscopy. Finally, we correlate physicochemical transformations with mechanical, adhesive and tribological properties of coating deposited by dip coating technique on stainless steel 430 and heat treated.

2. Experimental

2.1. Samples preparation

The substrate is AISI 430 ferritic stainless steel. Samples consist of plate 8×2 cm and 1 mm thick. Its average roughness (R_a), measured by White Light Interferometry is about 0.03 μm.

The precursors used were 3 glycidoxypropyltrimethoxysilane (GPTMS) and aluminum tri sec butoxide (ASB) [22]. GPTMS and ASB (80 wt.% in isopropanol) were mixed at room temperature. Water was added into the mixture. A precipitate was formed immediately. The precipitate was then peptized to a clear and transparent solution. The peptization time was approximately 30 min. The precursor solution was then aged for 24 h at room temperature. Each sample surface was cleaned and degreased in acetone. Then, a chemical pretreatment is needed before sol deposition, to improve coating adhesion. It was performed as follows: an immersion in a NaOH bath maintained at 60 °C, followed by a neutralization in an acidified solution of HCl at rooms temperature. Samples were finally washed in ethanol and dried in air. Then, Substrates were coated by dip coating (with a speed of 30, 50, 75 and 100 mm/min). Coatings were dried for 24 h at 50 °C

* Corresponding author. Tel.: +33 5 61 55 72 21.
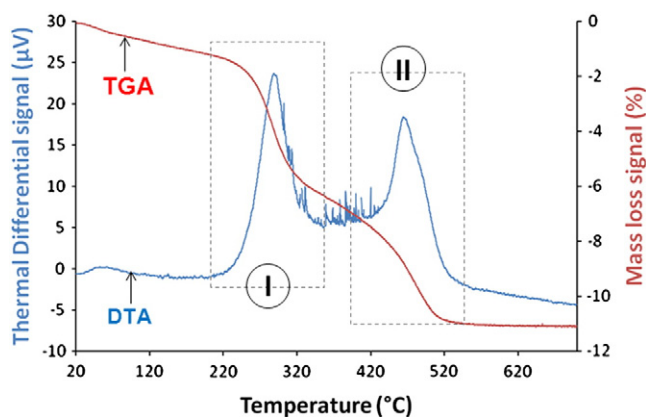 *E-mail address:* rahoui@chimie.ups-tlse.fr (S. Rahoui).

Fig. 1. Thermal analysis (TGA/DTA) curves for bulk xerogel (GPTMS and ASB precursors) in air atmosphere.

and then densified by thermal treatment for 16 h at different tempera tures (110, 200, 250, 300, 400 and 500 °C) with heating rate of 50 °C/h. Cooling rate is about 20 °C/h. Bulk xerogels were obtained using the sol prepared by the previously described synthesis but then dried and thermally treated in an alumina container.

2.2. Characterizations

Substrate's roughness was measured with a ZYGO white light interferometry.

Thermal properties of bulk xerogel were investigated by thermo gravimetric analysis (TGA) and differential thermal analysis (DTA) with a SETARAM TGDTA 92. The measurements were carried out in air, in the 20 °C 700 °C temperature range, with heating rate of 1 °C/min.

Microstructure, worn surfaces after tribological tests and thickness of coatings, were observed with a Scanning Electron Microscopy (SEM) JEOL JSM 35CF.

Structural analysis of xerogels thermally treated at different temper atures was performed with X ray diffractometer BRUKER D4 ENDEAV OR. XRD patterns were collected at room temperature by scanning steps of 0.02° (2θ) over a 10° < 2θ < 40° angular range and working with a Cu Kα radiation (0.15418 nm). RAMAN investigations were performed using a RAMAN microscope, HR HORIBA 800, equipped with red laser ($\lambda = 635$ nm) to restrict fluorescence.

Mechanical properties were evaluated with an Ultra NanoIndenter (UNHT, CSM Instruments). Elastic modulus and hardness were calcu lated with the method proposed by Oliver & Pharr [23]. Indentations were performed with a loading and unloading rate of 200 μN/min, and a maximum normal load of 100 μN. The Indenter was modified Berkovich, four indentations were performed on each sample. The thickness of samples tested is about 1.3 μm. Adhesive properties were evaluated by scratch test. A Nano Scratch tester (NST, CSM Instru ments) was used to measure critical loads of delamination. Nano scratch tests were performed with a loading rate of 80 mN/min, and a max load of 40 mN. Three scratches were performed on each sample.
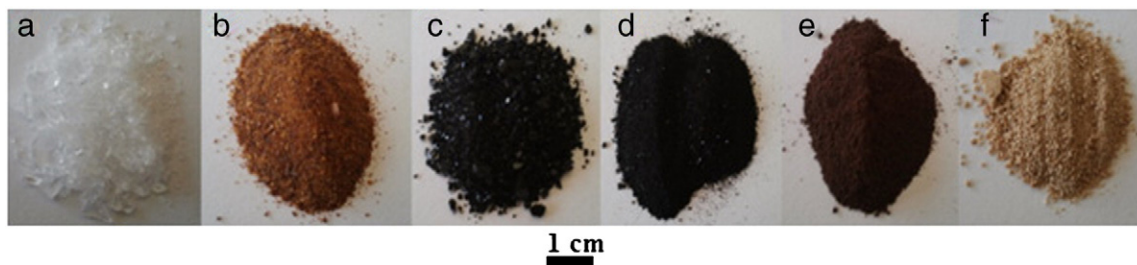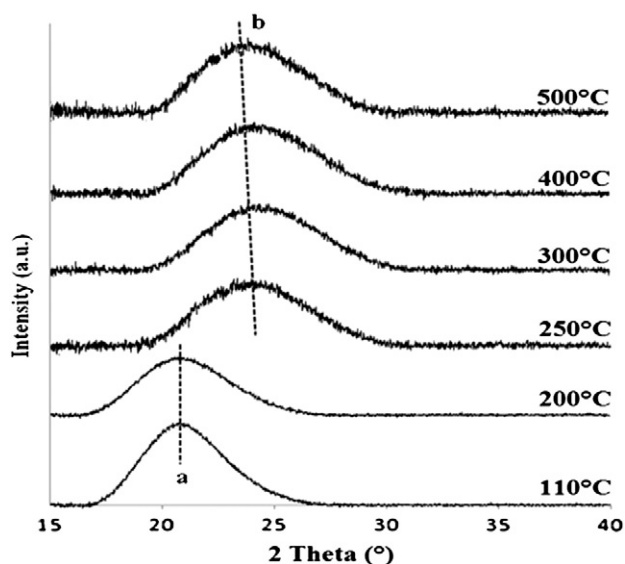

Fig. 3. X-ray patterns of the xerogel after heat treatment at 110, 200, 250, 300, 400 and 500 °C in air, during 16 h.

The tribological behavior of coated stainless steel were carried out on a linear ball/plane tribometer (CSEM Instruments), in ambient air and at ambient temperature. The pin was an alumina ball with a diameter of 6 mm. Loading force was 1 N and sliding distance was 6 mm (1 cycle corresponding to 12 mm). Sliding was performed at sliding velocity of 3.77 cm/s and test duration lasted for 1000 cycles. Three tests were performed on each sample.

3. Results and discussion

Before studying the effects of thermal treatments on mechanical and tribological properties of hybrid coatings deposited on 430 stainless steel, thermal behavior of xerogel was investigated by thermogravimetric and thermodifferential analyses (TGA DTA). The recorded curves report ed in Fig. 1 show, two exothermic peaks (DTA curve) and several domains of mass losses (TGA curve), illustrating physicochemical transformations thermally activated. The first mass loss below 200 °C is associated with the evaporation of solvents: water and alcohol. Beyond this temperature, two strong mass losses and two exothermic peaks appear. The first exothermic peak occurs in 220 350 °C temperature range (domain denoted I) and the second occurs in 400 550 °C temperature range (domain denoted II). Generally, polymeric materials are thermally decomposed around 250 °C [24 27]. So, reaction occurs in domain I, could be associated with thermal degradation of organic network.

Characteristic temperatures were highlighted with thermal analysis. In order to explain reactions occur in domain I and II, heat treatments were applied on bulk xerogel previously dried 24 h at 50 °C. Heat treat ments were carried out in air during 16 h, at 110, 200, 250, 300, 400 and 500 °C.
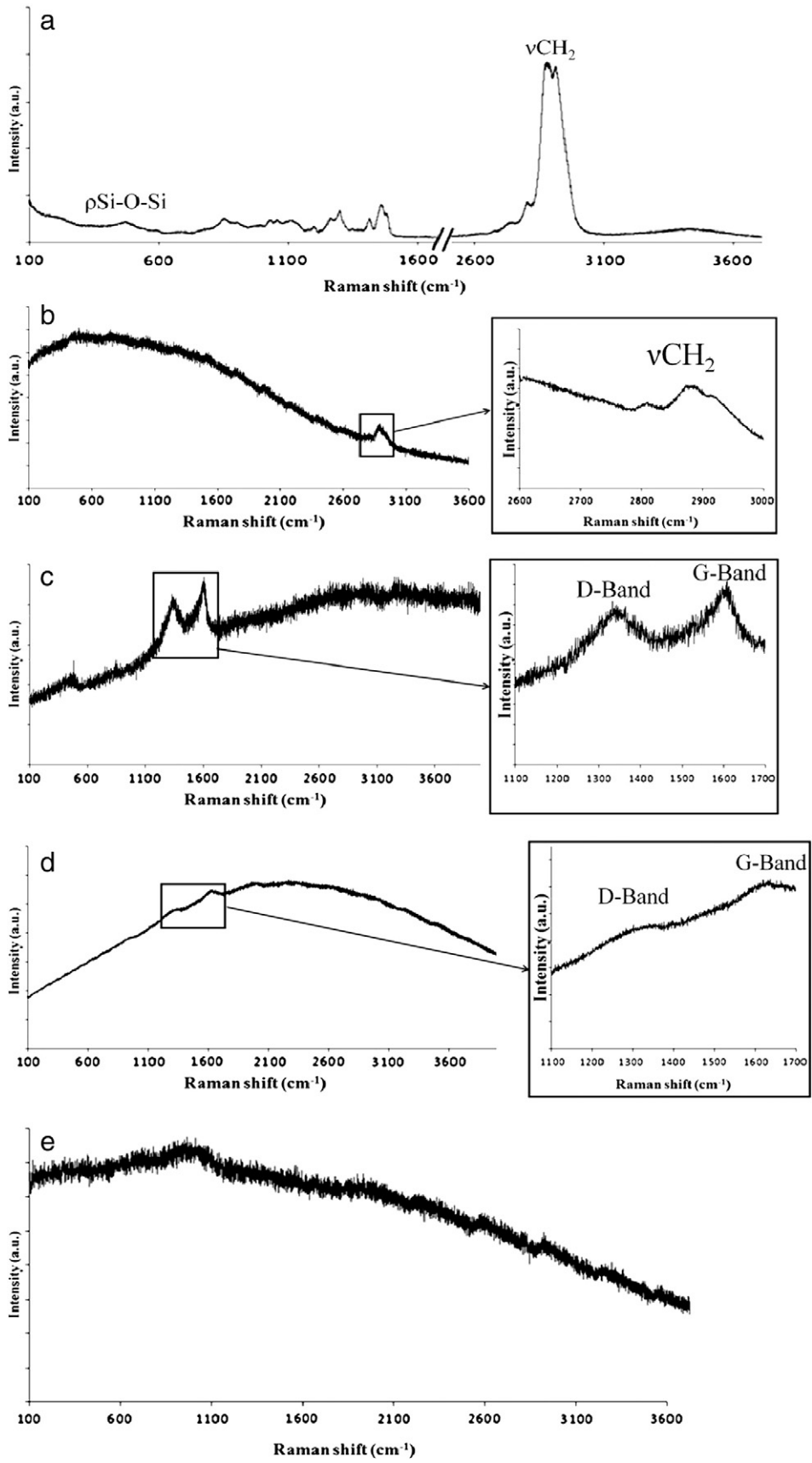

Fig. 2. Pictures of xerogel heat treated in air during 16 h at 110 (a), 200 (b), 250 (c), 300 (d), 400 (e) and 500 °C (f).

Fig. 4. Raman spectra of xerogel heat treated at different temperatures during 16 h in air: (a) 110 °C, (b) 200 °C, (c) 250 °C, (d) 300 °C and (e) 400 °C.

Table 1
Assignments of Raman vibrational modes of xerogel heat treated at 110 °C [31–33].

Vibrational mode assignments	Raman shift (cm^{-1})
Si–O–Si rocking	477
C–O–C + C–C stretching	857
CH_2 rocking	1040
CH_2 bending	1420
CH_2 bending	1465
CH_2 stretching	2810
CH_2 stretching	2890
CH_2 stretching	2920

The first observations were the color changes of the compounds after heat treatments, depending on the applied temperature (Fig. 2). After heat treatment at 110 °C, the xerogel was transparent. After 250 °C, it turned to black. Finally, after 500 °C, xerogel was brown. In order to correlate these color changes with thermal transformations of hybrid, we have first characterized each sample by X-ray diffraction and then by Raman spectroscopy. In Fig. 3 are reported X-ray diffraction patterns in the angle domain where diffraction signal appear. The low intensity and the widths of diffraction peaks indicate samples are amorphous. For the xerogel treated at 110 °C, the maximum of signal, denoted (a), observed around $2\theta = 20.4°$, is characteristic of hybrid organic inorganic [28,29]. Above 200 °C, the intensity of signal (a) decreases and signal disappears at 250 °C, due to the thermal decomposition of organic phase. This disappearance confirms thermal decomposition of organic network occurs in domain I. From 250 °C, another signal, denoted (b), appears around $2\theta = 23°$. This signal is attributed to the (101) of SiO_2 cristobalite [30].

XRD analysis confirmed reaction I is thermal decomposition of organic network, but it doesn't explain reaction II. We used Raman spectroscopy to follow structural evolution of bulk xerogel after heat treatment at different temperatures during 16 h in air. The Raman spectra of heated xerogel at 110, 200, 250, 300, 400 and 500 °C are respectively reported in Fig. 4a, b, c, d, e.

In Fig. 4a the Raman spectra of the heated xerogel is at 110 °C. The Raman bands with assignment of vibrational modes, are reported in Table 1. The peaks at 2810, 2890 and 2910 cm^{-1} are attributed to CH_2 stretching of organic network. The peak at 477 cm^{-1} is attributed to Si–O–Si rocking of inorganic network. At this temperature xerogel is hybrid. After heat treatment at 200 °C (Fig. 4b), despite the appearance of fluorescence, peaks of CH_2 stretching are still present, which means organic network is not yet thermally decomposed.

The Raman spectra (Fig. 4c) corresponding to the heated xerogel at 250 °C, pointed out two bands at 1346 cm^{-1} and 1606 cm^{-1}. These bands are characteristic of the presence of D Band due to Disorder and G Band for Graphite in amorphous carbon [34–39] resulting, in our case, in the thermal decomposition of organic groups of hybrid xerogel. After heat treatment at 300 °C (Fig. 4d), the two bands characteristic of
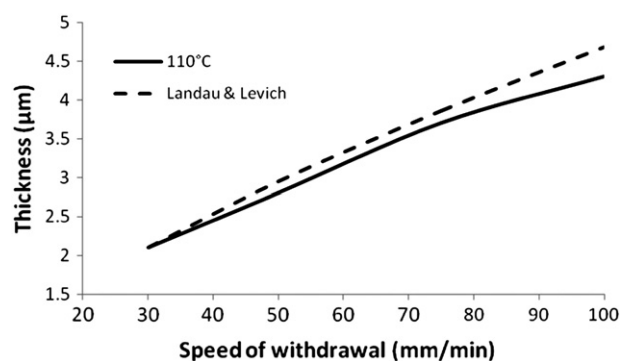

Fig. 6. Changes in thickness versus the withdrawal rate, for coating heat treated at 110 °C and Landau & Levich law [39].
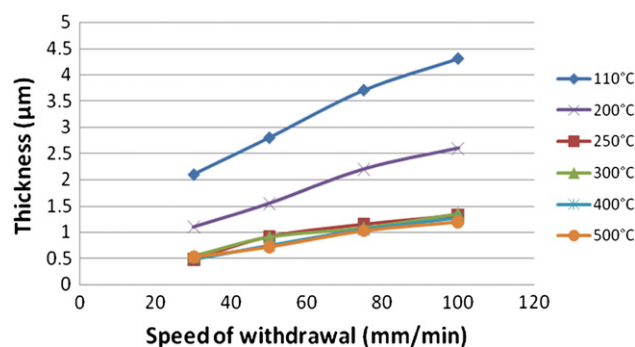

Fig. 7. Changes in coating thickness versus the withdrawal rate of dip-coating for different temperatures of heat treatment, 16 h, in air.

amorphous carbon are conserved, but the signal intensity is less apparent, because of fluorescence.

After heat treatment at 400 °C (in domain II), Raman spectra (Fig. 4e) shows no signal because of fluorescence (Raman spectra of xerogel heat treated at 500 °C is not shown because it presents no signal too). However, we can suppose, reaction II highlighted with thermal analysis could be attributed to the amorphous carbon oxidation.

After these preliminary experiments on xerogel and their thermal transformations, the sol was deposited on stainless steel substrate by the dip-coating process. We used several withdrawal rates (30, 50, 75 and 100 mm/min), to obtain coatings with various thicknesses. Then, coatings were heat treated at 110, 200, 250, 300, 400 and 500 °C in air during 16 h. Coatings thicknesses were measured from cross section observations by scanning electron microscopy (SEM). We have reported in Fig. 5 the cross section and surface observations by SEM of coating heat treated at 110 °C. Coating shows a good coverage and
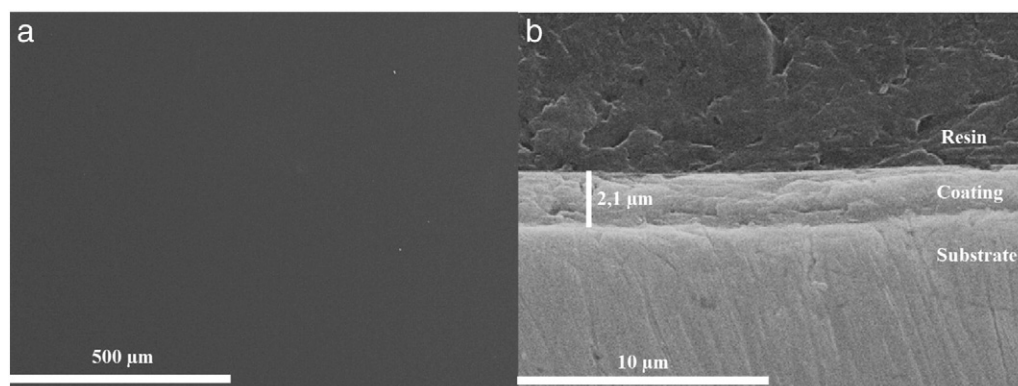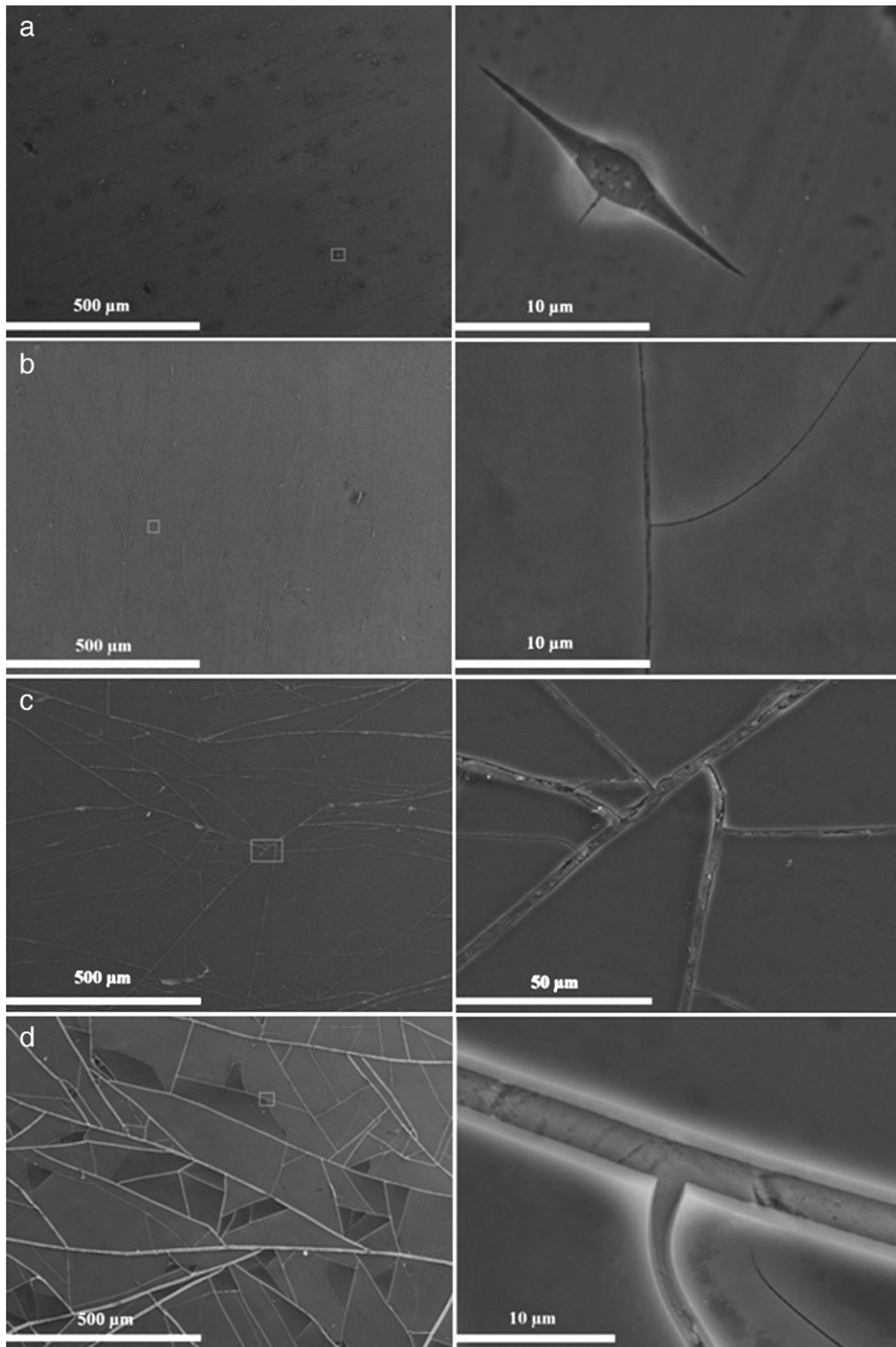

Fig. 5. SEM observations of surface (a) and cross section (b) of coating deposited by dip-coating at 30 mm/min, dried at 50 °C/24 h and heat treated at 110 °C during 16 h in air.

Fig. 8. SEM observations of surface of coating heat treated at 250 °C during 16 h in airs for different thickness; (a) 0.48 μm (b)0.98 μm (c) 1.15 μm (d) 1.32 μm.

we can notice the homogeneity of thickness and the apparent good adhesion of coating after the cross section preparation.

In Fig. 6, we observed that thicknesses of films were controlled with the withdrawal rate. The increase in thickness versus the withdrawal rate, is in good agreement with the Landau & Levich relation [40].

For each withdrawal rate, we have reported in Fig. 7 the evolution of thicknesses of deposits after heating at different temperatures. We can observe that beyond 110 °C, all the coatings decrease in thicknesses. Thickness reduction is about 50% after heat treatment at 200 °C and it's about 75% after 250 °C.

From SEM observations of the surfaces of heated samples, we have notice that the thermal treatments beyond 200 °C had some effects on the cohesion of deposits and these were depending on the thickness of them. For example, we can see in Fig. 8, that for a coating
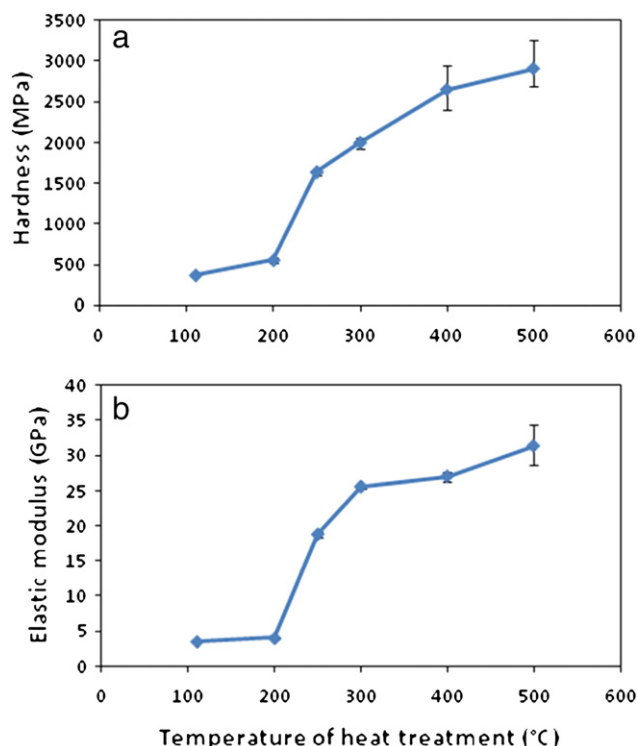
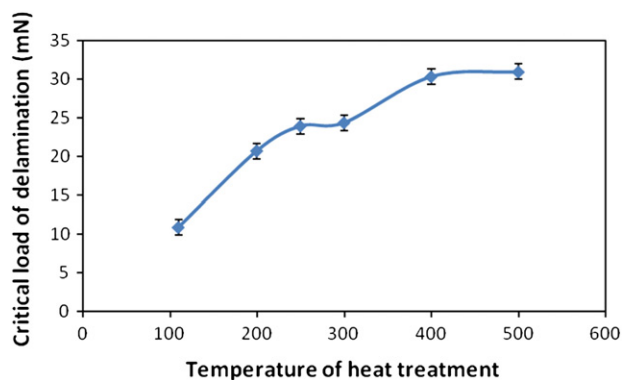**Fig. 9.** Values of hardness (a) and elastic modulus (b) as a function of temperature of heat treatment.

Fig. 10. Values of critical load of delamination as function of temperature of heat treatment.

deposited at 30 mm min^{-1}, small cracks appear after heat treatment at 250 °C and the size of them increase for the higher thicknesses. Indeed, for a thickness of 0.48 μm, we notice the presence of cracks of

short length (15 μm) which doesn't spread on the whole surface. In the case of larger thicknesses, cracks spread over the whole surface, which leads to the formation of platelets. Then, these platelets retract and extend the cracks. According to thermal analysis, the transformation of material at 250 °C causes mass loss, and leads to thickness reduction and cracking of coatings.

A theorical relation could estimate critical thickness of cracking h_c [41 43] for coating thermally treated at 250 °C during 16 h in air.

$$h_c \quad (K_{Ic}/\sigma)^2 \left(1/\Omega_c(\Sigma)^2\right) \tag{1}$$

K_{Ic} is the toughness of material constituting the coating. Its value is about 4 MPa m$^{1/2}$ in this study [44]. σ is the stress generated in the coating. In the case of elastical behavior law: σ = Eε. E is elastical modulus of coating and ε is the deformation.

$$\varepsilon \quad 1/3\log(\text{final thickness/initial thickness}).$$

$\Omega_c(\Sigma)$ depend on the stress generated in the coating and elastic modulus ratio between coating and substrate. Its value is about 1.5 in this study. So, we could calculate critical thickness of cracking for the coating thermally treated at 250 °C; hc ~ 0.77 μm. This estimating seems to be consistent with the values measured.

So, for heat treatment beyond 200 °C, we can correlate, thickness reduction of coatings and the cracks, probably resulting to the high strains of coatings during the decomposition of organic part of xerogel in oxidized phase of silicon with amorphous carbon. These transformations may cause changes in mechanical properties, so we have decided to check the evolution.

Fig. 9, shows the values of hardness (a) and elastic modulus (b) as a function of temperature of heat treatment. Applied load don't exceed 0.1 mN, in order to there is no contribution of the substrate on the measured values. Coatings heated at 110 and 200 °C have a similar value of hardness (~500 MPa) and elastic modulus (~5 GPa). Indeed, at theses temperatures coatings is hybrid and the values of hardness and elastic modulus correspond to the values comonly measured on hybrid organic inorganic coatings [14,45 48]. From 250 °C, appears a significant increase of hardness and elastic modulus. These results can be explained by the decomposition of organic network and the formation of oxydized silicon phase. The maximum values of hardness (2906 MPa) and elastic modulus (31.38 GPa) were measured for samples heat treated at 500 °C.

Then, we performed nanoscratch tests in the aim to study the change in adhesion properties of coated .stainless steel. Thickness of samples tested (~13 μm) and length of scratch (0,5 mm) was chosen in the aim to limit crack influence. The value of the critical load of delamination reported in Fig. 10 versus the temperature of heating, increases from 10.85 mN at 110 °C to 30.96 mN 500 °C. Even if, this increase is not simple to explain from the made experiments, we
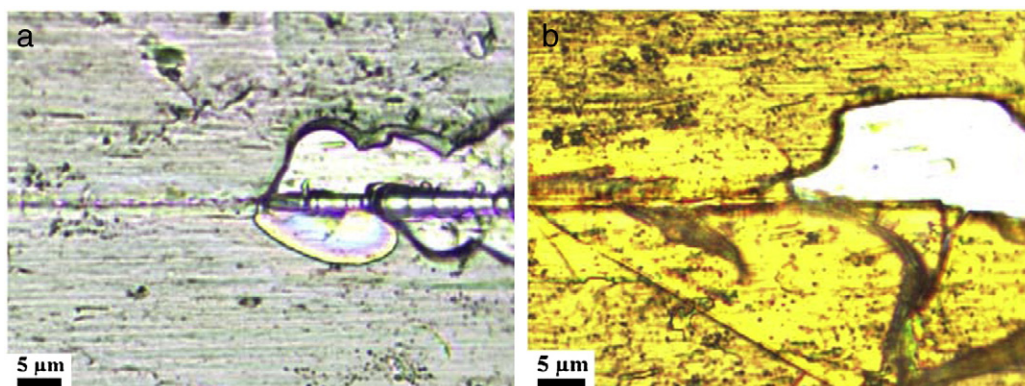
Fig. 11. Scratch patterns of coatings heat treated at 110 °C (a) and 250 °C (b).
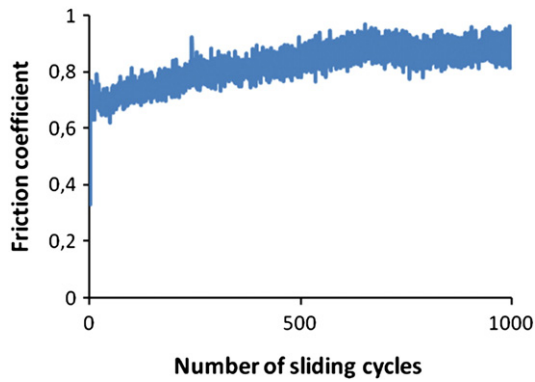
Fig. 12. Tribological property of uncoated substrate.

can notice here, that despite the cracks induced by the thermal transformation of xerogel, coatings keep a good adhesion on substrate. Observations of scratch pattern of coatings heat treated at 250 °C (Fig. 11), show delamination doesn't initiate on crevice.

Fig. 12 shows friction coefficient of substrate without coating as a function of sliding cycles. After 1000 cycles friction coefficient is about 0.8. Friction coefficients of coatings heat treated at different temperatures are reported in Fig. 13. All tests exhibit a good reproducibility. In the thickness range obtained (Fig. 7), it has no influence on tribological behavior of coatings. For example, Fig. 14 reports friction coefficients of coatings heat treated at 110 °C for different thickness. There are no significant differences between this four. Coatings heat treated at 110 °C and 200 °C (Fig. 13) present a similar tribological behavior. Friction curves present two steps. In the first step friction coefficient is about 0.5. From 400 cycles, friction coefficient increased to 0.8 until the end of test (1000 cycles). Average width of wear track measured after
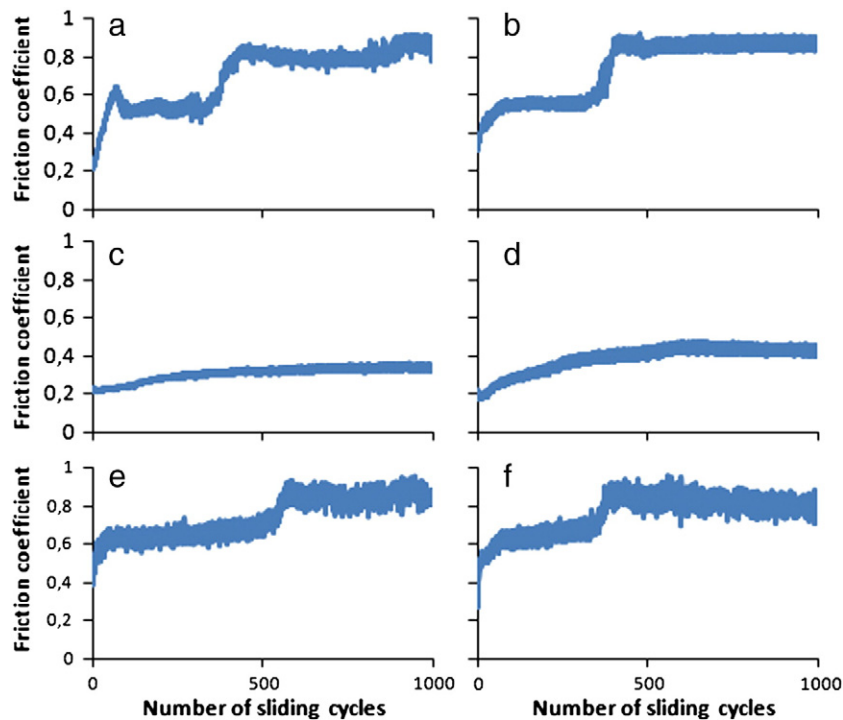

Fig. 13. Tribological properties of sol–gel coatings heat treated at different temperature: (a) 110 °C, (b) 200 °C, (c) 250 °C, (d) 300 °C, (e) 400 °C, and (f) 500 °C.
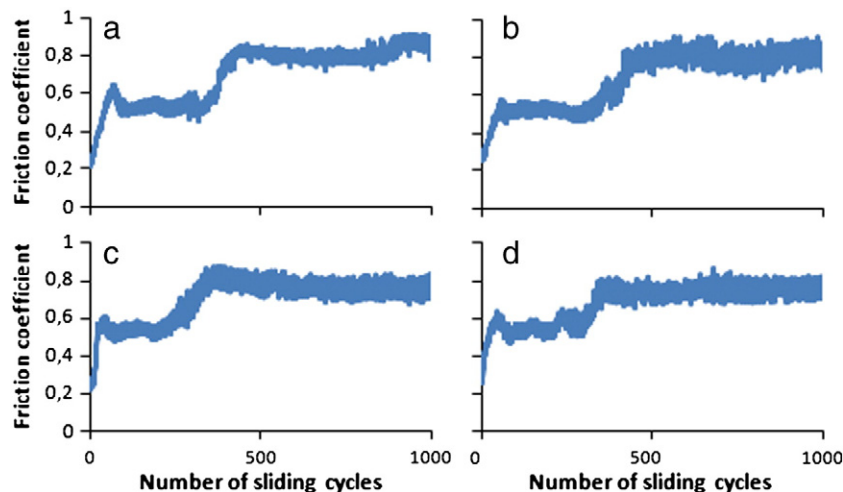

Fig. 14. Tribological properties of sol–gel coatings heat treated at 110 °C for different thickness: (a) 2.1 μm, (b) 2.8 μm, (c) 3.7 μm and (d) 4.3 μm.
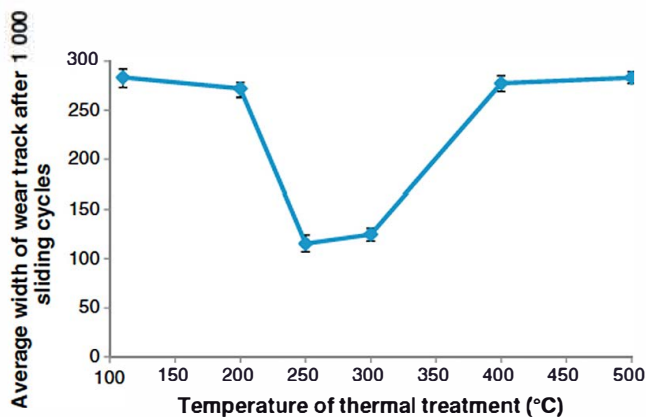
Fig. 15. Average width of wear track after 1000 sliding cycles versus temperature of heat treatment of coatings.

1000 cycles of sliding cycles (Fig. 15) is about 277 μm. Worn surface (Fig. 16) after 1000 cycles, show a large amount of debris accumulated around the worn track, indicating abrasive wear. After heat treatment at 250 °C or 300 °C (I), friction curves show a great reduction of friction coefficient to a value of 0.35. We also observe a reduction of average width of wear track to 120 μm. The transformation at 250 °C has improved significantly friction and wear. At this temperature, coating is no longer a hybrid, because of thermal decomposition of organic network. Raman spectroscopy revealed formation of amorphous carbon. Finally, after heat treatment at 250 °C, coating consists in amorphous carbon in oxidized phase of silicon, which shows better tribological behavior. Measurement of average width of wear track indicates wear is also reduced. Sliding curves of coatings heat treated at 400 and 500 °C (II), show tribological behavior close to the coatings heat treated at 110 and 200 °C. This increase in friction coefficient is probably induced by the oxidation from 400 °C of amorphous carbon pointed out by the exothermic phenomenon on DTA curve and the mass loss observed on TGA curve.

4. Conclusion

Organic inorganic coatings were deposited by dip coating onto stainless steel 430 and heat treated with different temperatures. The influence of temperature of heat treatment on the chemical and structural transformation of xerogel deposited were corelated to the mechanical properties and tribological behavior. The hybrid organic inorganic coating obtained from sol gel reaction and thermal treatment at 110 °C undergone at 250 °C a decomposition of organic groups. This transformation involves thickness reduction of coatings and cracks appear for the higher thickness of deposits. So, beyond 250 °C, coating is mainly an inorganic material and appears a significant increase in hardening but also a decrease in friction coefficient. We have shown from Raman spectroscopy that thermal decomposition of organic groups at 250 and 300 °C produces amorphous carbon in an oxyde matrix. The tribological tests of coatings heat treated at these temperatures show a significative decrease of the friction coefficient and wear. From 400 °C, the increase in friction coefficient is probably induced by the oxidation of amorphous carbon pointed out by the exothermic phenomenon and the mass load respectively observed on DTA and TGA curves.

In prospect, it would be very interesting to analyse the chemical and structural changes with NMR spectroscopy, and complete Raman spectroscopy with IR spectroscopy. Moreover, it would be interesting to study influence of parameters of heat treatment like the environnment or the duration.

References

[1] M. Gui, S.B. Kang, Mater. Lett. 51 (2001) 396–401.
[2] P.V. Ananthapadmanbhan, T.K. Thiyagarajan, K.P. Sreekumar, R.U. Satpute, N. Venkatramani, K. Ramachandran, Surf. Coat. Technol. 168 (2003) 231–240.
[3] H.K. Kang, S.B. Kang, Mater. Sci. Eng. A428 (1–2) (2006) 336–345.
[4] P. Fauchais, A. Vardelle, A. Denoirjean, Surf. Coat. Technol. 97 (1997) 66-78.
[5] U. Wiklund, M. Larsson, Wear 241 (2000) 234–238.
[6] C. Martini, L. Ceschini, Tribol. Int. 44 (2011) 297–308.
[7] P. Gupta, V. Singh, E.I. Meletis, Tribol. Int. 37 (2004) 1019–1029.
[8] P. Galliano, J.J. De Damborenea, M.J. Pascual, A. Duran, J. Sol-Gel Sci. Technol. 13 (1998) 723–727.
[9] D.C.L. Vasconcelos, J.A.N. Carvalho, M. Mantel, W.L. Vasconcelos, J. Non-Cryst. Solids 273 (2000) 135–139.
[10] P. Innocenzi, M. Esposto, A. Maddalena, J. Sol-Gel Sci. Technol. 20 (2001) 293–301.
[11] J. Ballarre, D.A. Lopez, N.C. Rosero, A. Duran, M. Aparicio, S.M. Ceré, Surf. Coat. Techol. 203 (2008) 80–86.
[12] M. Lechna, I. Holowacz, A. Ulatowska, H. Podbielska, Surf. Coat. Techol. 151–152 (2002) 299–302.
[13] F. Ansart, J.-P. Bonino, Ch. Robert, P. Lenormand, C. Viazzi, Key Eng. Mater. 529 (2006) 317–318.
[14] J.-B. Cambon, J. Esteban, F. Ansart, J.-P. Bonino, V. Turq, Mater. Res. Bull. 47 (2012) 3170–3176.
[15] K. Joncoux-Chabrol, J.-P. Bonino, M. Gressier, M.-J. Menu, N. Pébère, Surf. Coat. Techol. 206 (2012) 2884–2891.
[16] W. Liu, Y. Chen, G. Kou, T. Xu, D.C. Sun, Wear 254 (2003) 994–1000.
[17] W. Zhang, W. Liu, Q. Xue, Mater. Res. Bull. 36 (2001) 1903–1914.
[18] W. Zhang, W. Liu, C. Wang, Wear 253 (2002) 377–384.
[19] J.-B. Cambon, F. Ansart, J.-P. Bonino, V. Turq, Prog. Org. Coat. 75 (2012) 486–493.
[20] E. Certhoux, F. Ansart, V. Turq, J.-P. Bonino, J.-M. Sobrino, J. Garcia, J. Reby, Prog. Org. Coat. 76 (2013) 165–172.
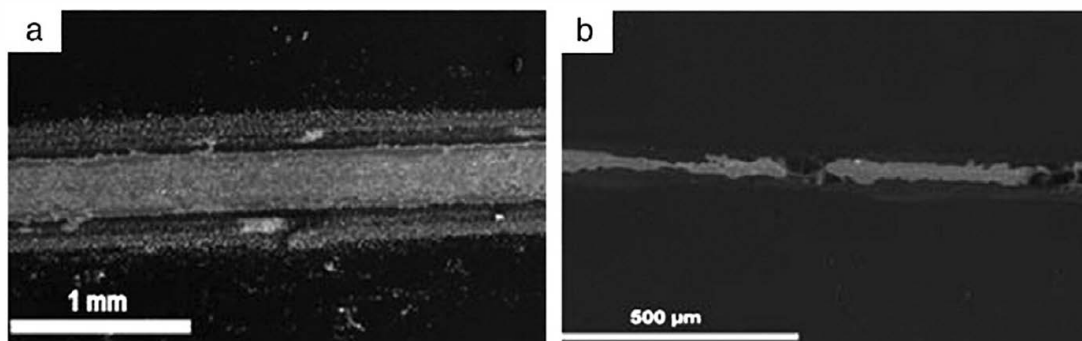[21] V. Meiffren, K. Dumont, P. Lenormand, F. Ansart, S. Manov, Prog. Org. Coat. 71 (2011) 329–335.

Fig. 16. Sem observations of worn surfaces after 1000 cycles of coatings heat treated at: (a) 110 °C and (b) 250 °C.

[22] J. Liu, J.C. Berg, J. Mater. Chem. 17 (2007) 4430–4435.
[23] W.C. Oliver, G.M. Pharr, J. Mater. Res. 7 (1992) 1564–1582.
[24] S.V. Levchik, G. Camino, M.P. Luda, L. Costa, G. Muller, B. Costes, Polym. Degrad. Stab. 60 (1998) 169–183.
[25] S.K. Poznyak, M.L. Zheludkevich, D. Raps, F. Gammel, K.A. Yasakau, M.G.S. Ferreira, Prog. Org. Coat. 62 (2008) 226–235.
[26] J. Macan, I. Brnardic, S. Orlic, H. Ivankovic, M. Ivankovic, Polym. Degrad. Stab. 91 (2006) 122–127.
[27] Y.L. Liu, W.L. Wei, K.Y. Hsu, W.H. Ho, Thermochim. Acta 412 (2004) 139–147.
[28] L. Shao, T.S. Chung, Int. J. Hydrogen Energy 34 (2009) 6492–6504.
[29] M.L. Chua, L. Shao, B.T. Low, Y. Xiao, T.S. Chung, J. Membr. Sci. 385–386 (2011) 40–48.
[30] J. Xu, S. Thompson, E. O'Keefe, C.C. Perry, Mater. Lett. 58 (2004) 1696–1700.
[31] H. Aguiar, J. Serra, P. Gonzalez, B. Leon, J. Non-Cryst. Solids 355 (2009) 475–480.
[32] D. Bersani, P.P. Lottici, M. Casalboni, P. Prosposito, Mater. Lett. 51 (2001) 208–212.
[33] H. Matsuura, K. Fukuhara, J. Polym. Sci. B 24 (1986) 1383–1400.
[34] F. Tuinstra, J.L. Koenig, J. Chem. Phys. 53 (1970) 1126–1130.
[35] A.C. Ferrari, J. Robertson, Phys. Rev. B 61 (2000) 075414, (13 pages).
[36] A.C. Ferrari, B. Kleinsorge, G. Adamopoulos, J. Robertson, W.I. Milne, V. Stolojan, L.M. Brown, A. Libassi, B.K. Tanner, J. Non-Cryst. Solids 266–269 (2000) 765–768.
[37] R.O. Dillon, J.A. Woollam, V. Katkanan, Phys. Rev. B 29 (1984) 3482–3489.
[38] S. Piscanec, F. Mauri, A.C. Ferrari, M. Lazzeri, J. Robertson, Diamond Relat. Mater. 14 (2005) 1078–1083.
[39] C. Pardanaud, E. Aréou, C. Martin, R. Ruffe, T. Angot, P. Roubin, C. Hopf, T. Schwarz-seling, W. Jacob, Diamond Relat. Mater. 22 (2012) 92–95.
[40] L. Landau, B. Levich, Acta Physicochim. URSS 17 (1942) 42.
[41] M.S. Hu, M.D. Thouless, A.G. Evans, Acta Metall. 36 (1988) 1301–1307.
[42] G. Gille, Thin Solid Films 111 (1984) 201–218.
[43] S. Bec, A. Tonck, J.-L. Loubet, MRS proceedings, 308, 1993, p. 577.
[44] M.F. Ashby, D.R.H. Jones, Engineering Materials 1: an Introduction to Properties, Applications and Design: v. 1, Butterworth-Heinemann Ltd., 2005
[45] A. Ferchichi, S. Calas-Etienne, M. Smaihi, P. Etienne, J. Non-Cryst. Solids 354 (2008) 712–716.
[46] A.J. Atanacio, B.A. Latella, C.J. Barbé, M.V. Swain, Surf. Coat. Technol. 192 (2005) 354–364.
[47] S. Yaacoub, S. Calas, J. Jabbour, R. Tauk, D. Zaouk, A. Khoury, P. Etienne, J. Non-Cryst. Solids 358 (2012) 3036–3041.
[48] C.A. Avila-Herrera, O. Gómez-Guzmán, J.L. Almaral-Sánchez, J.M. Yáñez-Limón, J. Muñoz-Saldaña, R. Ramírez-Bon, J. Non-Cryst. Solids 352 (2006) 3561–3566.